Final report

1. Project details

Project title	SOFC Accelerated, Development to Accelerate Field Demonstrations
Project identification (program abbrev. and file)	SOFC Accelerated, 64012-0225
Name of the programme which has funded the project	EUDP
Project managing company/institution (name and address)	Technical University of Denmark Anker Engelunds Vej 1 Building 101A 2800 Kgs. Lyngby Tel +45 45252525 Wolff-Ragnar Kiebach, woki@dtu.dk, +4546775624
Project partners	DTU Energy Conversion Haldor Topsoe A/S
CVR (central business register)	30 06 09 46
Date for submission	July 31, 2015

2. Short description of project objective and results

The original project aimed at enabling larger SOFC field demonstrations. During the project Topsoe Fuel Cell A/S (TOFC) closed down as a company. The project was continued under DTU management and Haldor Topsøe A/S (HTAS) joined as partner with commitment to contribute to the solid oxide electrolysis cell (SOEC) development. The original aims in WP1, WP2 and WP3 of the "SOFC accelerated" project, were not continued since the SOFC market situation has changed and is considered too far into the future at the moment. The focus of the remaining project period was on the continuation of selected tasks in WP4 and WP5 of strategic importance to DTU and of high relevance to SOEC development at HTAS in the originally anticipated timeframe.

Significant progress was made on the manufacturability of stacks and cells, a result which is now utilized in SOEC technology at HTAS. All promised milestones and deliverables were fulfilled and a technology transfer from SOFC to SOEC was successfully executed. From a future research perspective, several new concepts were developed and tested successfully as "proof-of-concept". In this context the development of net shaped cells, impedance on stack level and high performance SOEC cells should be outlined – these promising activities are planned to be continued and utilized in future national and international research/demonstration projects.

3. Executive summary

In light of promising results obtained on improved cells and stack components, activities in the project were continued to consolidate these developments which will help bringing SOFC/SOEC technology closer to market. The aim in the remaining project period was a technology transfer from SOFC to SOEC and to prove that results obtained can be developed further and utilized.

Significant progress was made on the manufacturability of stacks and cells, a result which will serve the SOEC applications. All project targets were met in the reporting period. Tasks selected for continuation were successfully completed and it was clearly shown that obtained results are can be utilized for SOEC application and are highly relevant for future research.

4. Project objectives

The original success criteria were modified and milestones were set to prove that results obtained in the first part of the project can be used and further developed for utilization in SOEC technology.

To summarize, we can conclude that:

1) The initial degradation behavior of the stacks in SOEC mode was successfully measured and analyzed. Developed stacks perform well in SOEC operation and implementation in commercial CO units developed by HTAS is possible. A HTAS stack with the latest design was further characterized using impedance spectroscopy. (Milestone 1)

2) Based on the long-term tests in various gas atmospheres, some of the developed steel and coatings solutions proved to be promising for SOEC applications, but implementation is not planned at this stage. (Milestone 2)
3) By the time of writing, stack yield at HTAS is above 75%, based on quality assurance criteria defined as a part of this project. This exceeds the project goal of 65 %. (Milestone 3)
4) Fully functional net shaped cells can be manufactured without additional shaping steps (Milestone 4).
5) The mechanical properties of the novel cathode backbone cells were found to be comparable to the standard DTU/HTAS cells (Milestone 5).
6) The new cathode backbone cell concept proved to have very high performance and to be very stable at high current densities. At the time of writing these cells are considered "world record" cells due to the low degradation rates observed in long-term tests (Milestone 6).

5. Project results and dissemination of results

5.1 WP 4 "Stacks"

Overview milestones and deliverables in WP4. Deliverables already delivered and reported before change in the project structure due to TOFC closure are marked in **black**; deliverables (including new and modified ones) relevant for this reporting period are marked in **green**.

WP 4	
Deliverables (including modified and new ones)	
4.1.1	Stack lifetime-limiting factors and recommendations (Report M9) **Delivered** Comparable deliverable for SOEC applications added (New deliverable 4.1.3)
4.2.1	Stack Robustness limiting factors and accelerated test (M9) **Delivered**
4.2.2	Recommendations to selected major robustness issues occurring under SOEC operation (Report M30) (**Modified)** **Delivered**
4.3.1	Campaign 1 stacks (Prototype series M9) **Delivered**
4.3.2	Analysis of campaign 1 yield, quality and process control (Report) **Delivered**
4.3.3	Campaign 2 stacks (Prototype series M18) **Delivered** Comparable deliverable for SOEC stacks added (New deliverable 4.3.7)
4.3.4	Analysis of campaign 2 yield, quality and process control (Report M20) **Delivered** Comparable deliverable for SOEC stacks added (New deliverables 4.3.8)
4.3.5	Evaluation of acoustic emission: A potential in-situ diagnostic tool in HTAS pilot production (Report M24) **Delivered**

4.4.1	Interconnect steel and coating solution suitable for SOEC application (Report M28)(**Modified)** **Delivered**
New deliverables from DTU	
4.1.3	Stack lifetime-limiting factors for SOEC applications identified (Report M30) **Delivered**
4.1.4	Evaluation of impedance spectroscopy as potential in-situ diagnostic tool for SOEC (Report M24) **Delivered**
4.1.5	Evaluation of impedance spectroscopy on full size TSP-1 stacks (Report M28) **Delivered**
4.4.2	Stability of developed EPD coating demonstrated under SOEC conditions (Report M26) **Delivered**
4.4.3	Performance of cheap alloys (ASIS 430, ASIS 441) under SOEC condition evaluated (Report M30) **Delivered**
New deliverables from HTAS	
4.3.7	Campaign 3: SOEC stacks (Prototype series M28) **Delivered**
4.3.8	Analysis of campaign 3 yield, quality and process control of SOEC stacks (Report M30) **Delivered**
4.3.9	TSP-1 stack for impedance measurements manufactured and delivered to DTU (prototype stack, M24) **Delivered**
4.4.4	50 Co-plated interconnects delivered to DTU for corrosion testing in SOEC relevant conditions (Prototype inter connects, M22) **Delivered**
4.4.5	Alloy ZMG23G10 with and without Co coating send to DTU (Coated interconnect steels M22) **Delivered**
New Milestones for work package 4	
M1	Title: *Initial degradation in SOEC stack studied with impedance spectroscopy*. Description: For SOEC stacks an initial degradation can occur in the first few hundreds hours of operation. The underlying degradation mechanism will be studied in detail using impedance spectroscopy. Time: M 26. **FULFILLED**
M2	Title: *Interconnect steel and coating solution developed at DTU and standard coating used at HTAS tested > 1000 h under SOEC operation conditions*. Description: Coated steel will be exposed to SOEC relevant conditions (a) pure oxygen; (b) H_2O/H_2 for > 1000 h at relevant temperatures. Results, including post mortem analysis, will be compared and recommendation for SOEC application will be made. Time: M30. **FULFILLED**
M3	Title: *Production yield of SOEC stacks produced in campaign #3 at HTAS is above 65%.* Description: Achievements obtained at TOFC for SOFC stacks will be transferred and retained at HTAS for SOEC stacks. Time: M28. **FULFILLED**

4.1 Development and production of SOEC stacks at HTAS

Improved stack design *(relevant to D4.3.7, D4.3.8, D4.3.9 and M3)*

Summary: A new and improved stack design (TSP-1) has been developed at HTAS. The new design has been implemented in production with a promising yield of 75%. A TSP-1 stack was delivered for impedance spectroscopy testing at DTU.

During the project period, a new stack design called TSP-1 was developed at HTAS. Compared to the previous "Delta" design, the new design includes an increased number of cells (thus more power), a simplified air manifold design, as well as improved flow distribution (Fig. 4.1). Furthermore, the new design can be handled without external compression and is packaged in a mechanically robust metal casing.

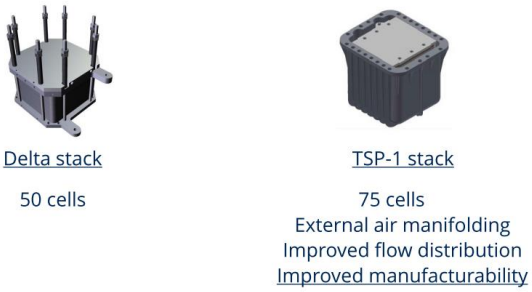

Figure 4.1: Comparison of HTAS's old (Delta) and new (TSP-1) stack designs.

The manufacturability of the new stack design was put to test in Campaign 3 of this project, which resulted in a stack production yield of 75%, thus satisfying the project milestone set at 65%. Comparing data from Campaigns 1 to 3 reported in this project, all key stack quality parameters (stack voltage at standard operating points, gas tightness, etc.) have seen steady improvements. Further improvements to both stack design and production yields are possible and are being pursued by HTAS outside of the concluding project.

4.2 Testing of HTAS stacks at DTU

Evaluation of impedance spectroscopy as potential in-situ diagnostic tool for SOEC *(relevant to D4.1.4, D4.1.5, D5.1.6 and M1)*

Summary: The degradation of an SOEC stack operated at 800 °C for 1000 h in CO/CO_2 electrolysis was successfully investigated by impedance spectroscopy. Gas phase impurities were identified as main reason for the observed initial degradation. Additionally, the possibility of recording impedance spectra on the new TSP1 stack design was evaluated. The quality of the obtained spectra was surprisingly high and exceeded expectations.

The 17-channel electrochemical impedance analyzer was upgraded to be able to operate in electrolysis mode, allowing currents of up to 100A at a maximum voltage of 60V. This is sufficient to operate full-sized TOFC/HTAS SOC stacks with up to 30 cells at current densities up to 1 A/cm^2. The quality of the measurements was confirmed by recording impedance spectra with fuel compositions reaching from pure steam to pure carbon dioxide electrolysis. The results are shown in Figure 4.. The spectra are of the same excellent quality as under SOFC conditions. The deviation of the measured imaginary parts of the spectra

and the ones derived by the Kramers Kronig theorem are below 0.5% which is DTU Energy's threshold for very good quality on stack level.

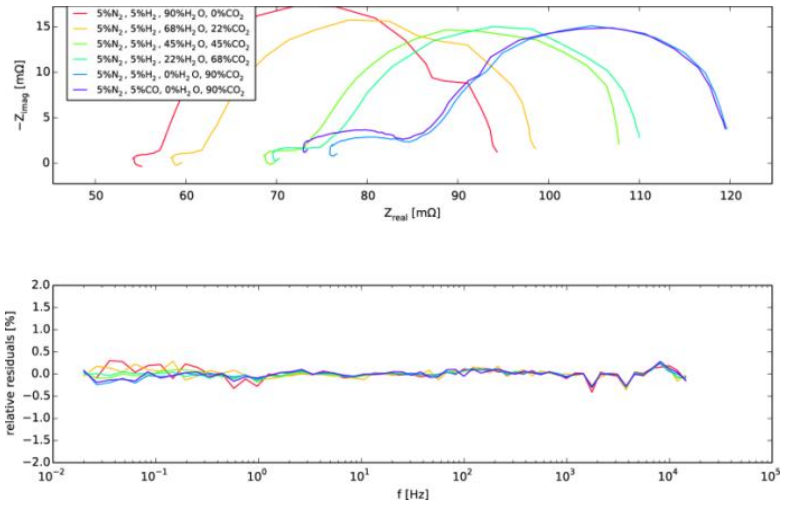

Figure 4.2: Quality of SOEC impedance spectra; top: spectra recorded with different fuel compositions; bottom: residuals of KK-test (<0.5% considered as excellent quality)

After the initial validation of the test setup, a degradation study was carried out. The test stack K-748 provided by TOFC/HTAS was a 14-cell stack with Delta design. The cells 5, 6, 9 and 10 were from a single batch of sprayed, the rest from a single batch of multi-layer tape casted cells (current manufacturing process).

The test was run for ~1000 hours at 800°C, 25A (~0.3 A/cm^2) with a fuel utilization of 50% and a fuel mixture of 5% nitrogen, 5% hydrogen and 90% carbon dioxide. Due to technical problems about 300 hours into the test only the results of the last 700 hours are shown.

Figure 4.33a shows the temporal development of the impedance spectra of the whole stack. The stack showed a clear increase of the electrode resistance (high frequency arc on the left-hand side). This was as well the case for the individual cells (not shown).

Figure 4.3b shows the single cells' average electrode resistance (blue dots), a band of confidence (single cell electrode resistance average plus/minus the standard deviation, green) and the stacks electrode resistance divided by the number of cells (red).

The width of the confidence band and therefore the relatively large standard deviation is most likely due to inductance artifacts from the wiring to the individual cells. Despite this, the stack's electrode resistance (divided by the number of cells) is in a very good agreement with the average cell resistance. It should as well be noted that the resistance of the state-of-the-art stack is very small. Therefore even small artifacts show a large effect.

The steady increase in resistance can be attributed to impurities in the supplied gasses. A similar process to the known initial degradation in fuel cell mode, caused by coarsening of the nickel particles, can be excluded. The latter phenomenon originates from the high nickel mobility in a steam rich atmosphere and is not present under the test conditions.

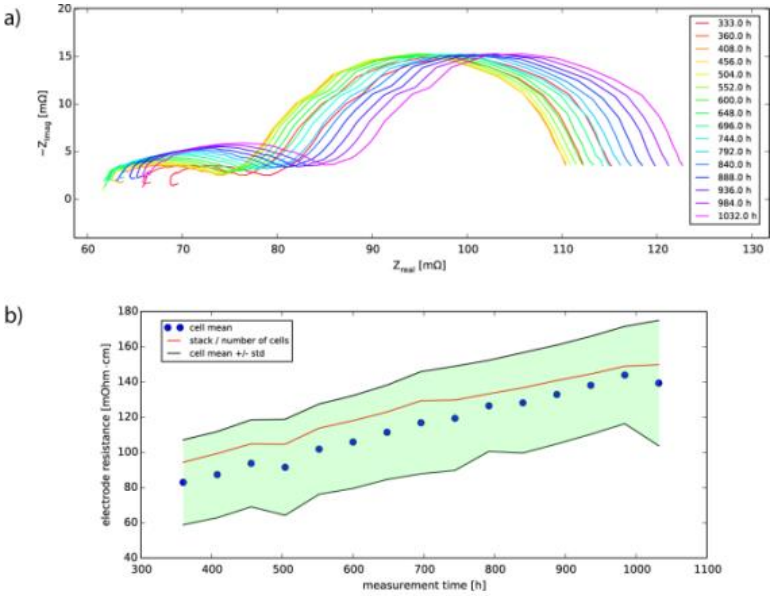

Figure 4.3: Degradation of stack K-748 under SOEC conditions; a: temporal development of stack impedance spectra over time; b: comparison of cell and stack electrode resistance (high frequency impedance)

At the end of the degradation test a significant decrease of the open circuit voltage (OCV) of the sprayed cells was observed. The difference to the worst new generation multi-layer tape casted cell was between 70 and 110mV and pointed to a strongly increased gas leakage between fuel and air side for the sprayed cells.

With HTAS's change from the Delta to the TSP-1 platform, the quality of the electrochemical impedance spectra needed to be re-evaluated. The previously used Delta stacks used for impedance measurements were special stacks modified to minimize inductance artifacts in the impedance spectra. For the TSP-1 platform, the goal was to move away from building special stacks (just for the purposes of impedance spectroscopy) to testing standard production stacks,. In order to assess the possibility of recording impedance spectra on the standard TSP-1 stack, an eight cell stack (Q-675) equipped with voltage probes on each interconnect was tested under similar SOEC conditions as the Delta stack K-748. The comparison of the impedance spectra is shown in Figure 4.4.

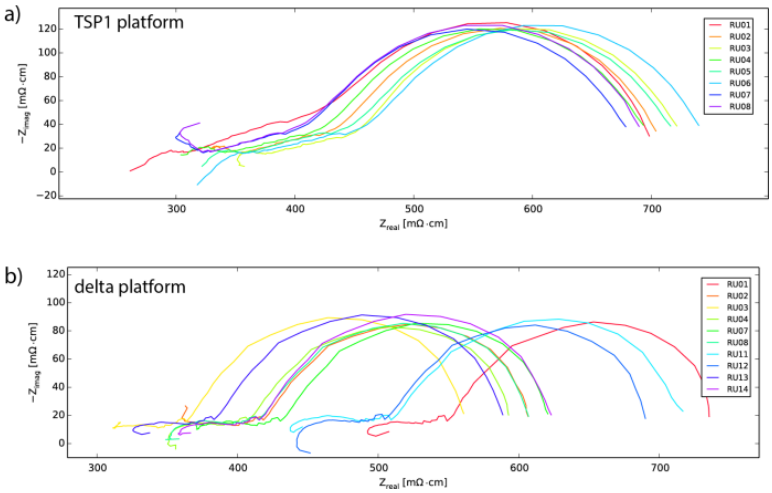

Figure 4.4: comparison of TSP-1 (a) and delta (b) platform impedance measurements

Due to the non-optimized configuration the TSP-1 stack impedance spectra show larger induction artifacts at higher frequency (left-hand side of the spectra) compared the delta stack. The magnitude of the inductance is nevertheless surprisingly low. It should as well be noted that the spectra were recorded right after starting up the stacks when the electrode resistance (high frequency) is very low. As the stack degrades, the high frequency resistances will become more prominent (see Figure 4.3) and the inductance artifacts less dominant.

It is still highly recommended to improve the TSP-1 platform's impedance response according to the experiences from the Delta design.

4.2 Stack robustness and lifetime (relevant to D4.1.3 and D4.2.2)

Summary: a list of stack lifetime-limiting factors as well as a list of improvements to major robustness issues has been compiled. These shortlists are considered as a good starting point for further cell, stack, and interconnect improvements to be pursued in the future.

Based on experiments performed at DTU and HTAS, the following factors are considered lifetime-limiting for cells and stacks operating in electrolysis mode:

1. Degradation of fuel electrode microstructure
   Changes in the structure of the Ni/YSZ fuel electrode are considered as the main cause for the degradation in the novel cells developed in WP5 (the rapid initial degradation in Fig. 5.7) and in the degradation observed in some stack tests.
2. Gas-phase impurities
   Gas-phase impurities seem to be just as detrimental to cells and stacks running in electrolysis mode as they are to cells and stacks running in fuel cell mode. An example of the negative effects of gas-phase impurities is shown in Fig. 4.3.
3. Interconnect corrosion
   Corrosion of the metallic interconnect and the accompanying increase in resistance remains as one of the critical lifetime-limiting factors for stacks.
4. Contacting / current distribution in stacks
   The in-plane distribution of current as well as the robustness of mechanical contact between cells and interconnects needs to be improved.

Based on experiments performed at DTU and HTAS, the following improvements for cells and stacks operating in electrolysis mode are proposed:

1. Cells with improved fuel electrode microstructure
   The structure of the Ni/YSZ fuel electrode could be re-designed to prevent or alleviate the detrimental microstructural changes observed in cells today.
2. Map out the effect of impurities on stack level
   In order to be able to improve the tolerance of an SOEC stack towards gas-phase impurities, the effect of impurities first needs to be quantified and mapped out on stack level.
3. Interconnect solutions for electrolysis operation
   Current interconnect and protective coatings have been designed with SOFC operation in mind. The best steel and coating solutions for SOEC operation may differ significantly from the solutions used today.
4. Improved current distribution
   One way to achieve better current distribution in stacks is to improve the air-side contact layer in cells. A potential solution using infiltration has been proposed and successfully tested in this project (see Section 5.3).

4.3 Probing the mechanical properties of stacks

Evaluation of acoustic emission: A potential in-situ diagnostic tool in HTAS pilot production (relevant to D4.3.5)

Summary: The acoustic emission during the production of 20 stacks at HTAS was recorded. Here only small correlation between stack integrity and quality during the production could be made. An optimized setup (microphone position and frequency range) at DTU showed a very clear correlation between stack failure and distinct acoustic signals.

Stack production at TOFC/HTAS was monitored by acoustic emission (AE) sensors (piezo-electric sensors).
Two types of sensors were installed on the top of the pushing rods at each of the 4 positions in the stack furnace (Figure 4.2a). These positions were chosen to be the least possible intrusive in the stack production and to keep the sensors at room temperature.
During the time the sensors were on the stack furnace, the conditioning and reduction of 20 stacks was recorded. Four of the monitored stacks, and potentially two others developed cell cracks during conditioning and reduction.
In Figure 4.2b, the amplitude of the recorded hits is reported for each sensor position together with a measure of the temperature. The signal recorded on the Pico sensors (on the side) mainly corresponds to friction of the piston (especially during unloading). Therefore, only the hits recorded by the Micro sensors (on top of the pushing rods) were reported in Figure 4.2b. It is to be noted that some of the sensors were unplugged when the set-up was dismounted (e.g. Micro sensors in stack position 1 and 2).

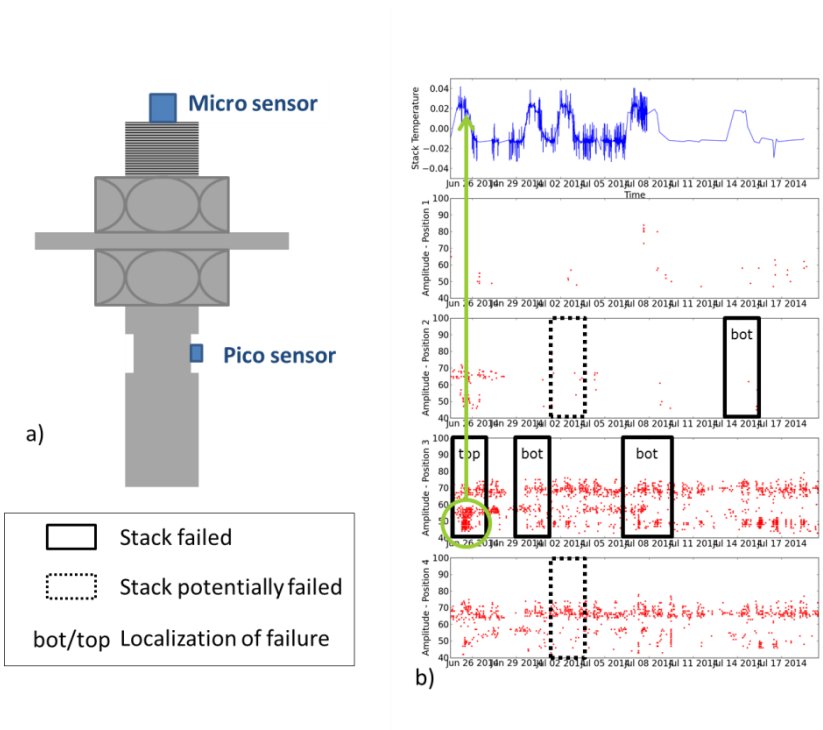

Figure 4.2 – Schematic positioning of the sensors at the top of the pushing rods (a) and amplitude of the signal recorded by the Micro sensors on each stack position (b)

Among the hits recorded, it is possible to exclude the hits of amplitude 60-80, which give a repetitive pattern corresponding to the working days. Except from that, no strong correlation between AE signal and stack failure could be detected, except for the stack broken on top (Figure 4.2b, position 3, run 1). For this stack, a concentration of hits of amplitude 40-60 occurred during stack reduction. For stacks broken at the bottom, the signal was probably damped by the stack.

Based on these experiences, stacks tested at DTU were investigated with optimized setup/microphones. More sensors were mounted in the stack test setup at various locations. Similar to previous reported results on stacks investigated at DTU, the hits recorded correlate very well to events in the stack (Figure 4.3), especially temperature variations, hydrogen/air flow variations, impedance measurements and piston removal, underlying the reproducibility and reliability of this method.

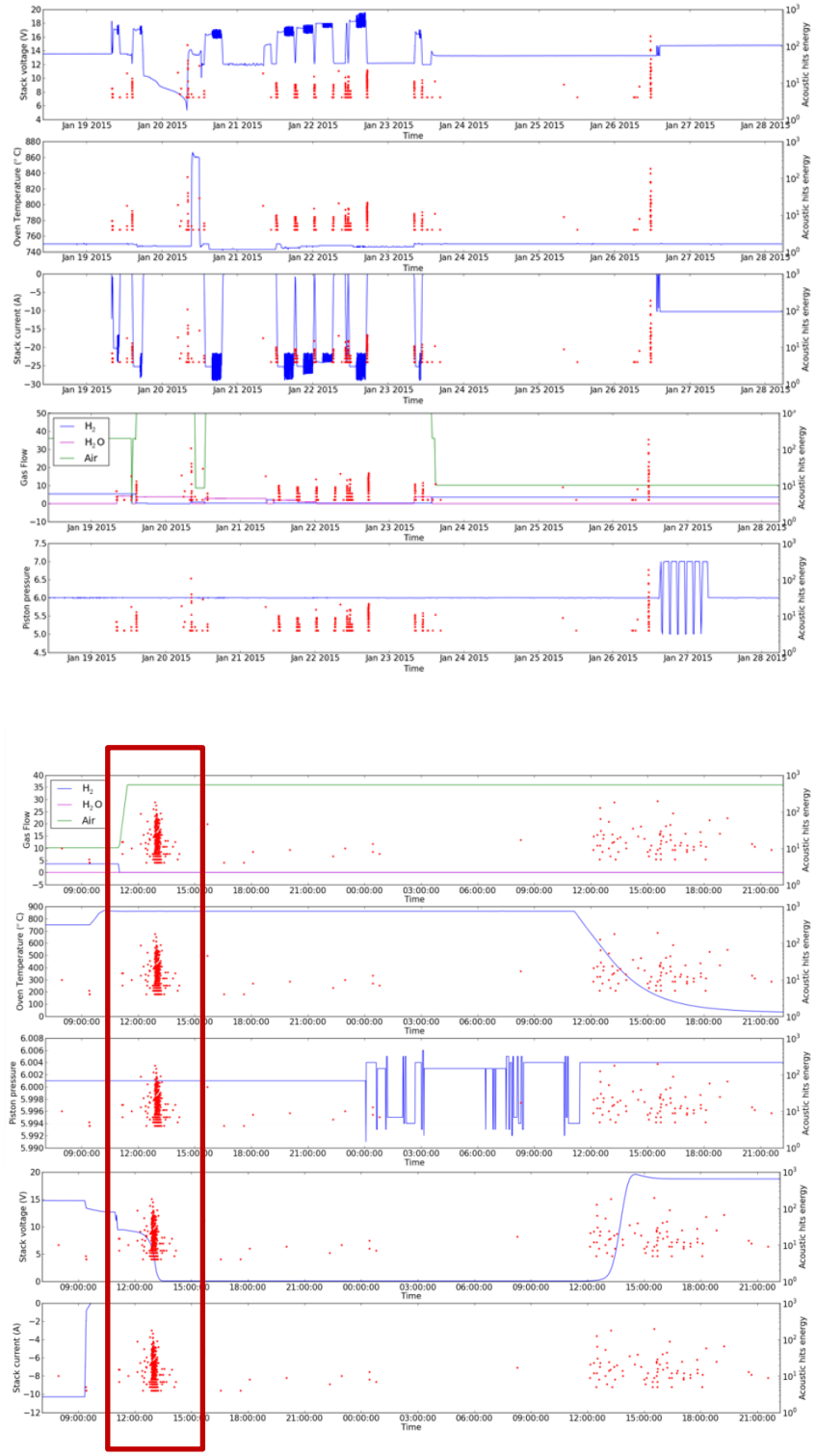

Figure 4.3 recorded hits as a function of events in the stack

At the end of the testing period, the cells in the stack were intentionally broken and very distinct and intense signals were recorded (red box in figure 4.3). These results show that acoustic emission can be used

as potential in-situ tool during stack production and operation if the sensors are located close enough to the stack and at the right stack positions.

It is therefore recommend to modify the production furnaces at HTAS accordingly (if possible) and to monitor stack production again.

4.4 IC steel and coating development

Summary: Electrophoretic deposition (EPD) as low cost coating technique was developed. The corrosion kinetics and area specific resistance (ASR) of uncoated and $Mn_{1.5}Co_{1.5}O_4$ coated (using EPD) commercial alloys (430 and 441) was evaluated and compared with standard Crofer alloys at relevant SOFC/SOEC operating conditions. For the anticipated low temperatures the commercial alloy 430 can be an interesting and cheap alternative for Crofer.

Coating development (relevant to 4.41, 4.4.2, 4.4.3 and M2)

Interconnect plates, made of ferritic type stainless steel, are widely used in planar solid oxide fuel cell (SOFC) or electrolysis cell (SOEC) stacks. These interconnect plates serve as current collector and separator for the neighboring fuel and oxygen electrode compartments of two adjacent cells. An intimate contact between the cell component and the interconnect (IC) plate is therefore essential to ensure optimum cell and stack performance.

The EPD process has been developed and improved for applying protective layers on SOFC/SOEC metallic interconnects. In order to control/improve the corrosion behavior of cheaper alloys, layers of protective coatings were modified via impregnation and co-deposition during the EPD process. A uniform coating of Mn-Co spinel was obtained in form of a porous layer. Addition of sintering aids such as Nb, Cu, Mn and the addition of reactive rare earths elements such as Y, Ce, La along with Mn-Co spinel was investigated and compared to commercial Mn-Co spinel coating from Fuel Cell Materials. Results showed that the addition of sintering aids and reactive elements to the spinel coating lead to a better densification and reduced the corrosion rate.

Oxidation kinetics of interconnect alloys (relevant to 4.41, 4.4.2, 4.4.3 and M2)

The chosen commercial low Cr ferritic stainless steels – 430 and 441 alloys – were compared against the specialty alloy Crofer 22APU, which is currently used as standard interconnect material. Air, pure oxygen and humidified hydrogen were chosen as relevant atmosphere for SOEC operation.

As expected, the corrosion rate at 800 °C of the uncoated commercial alloys are higher than the Crofer alloys, as these alloys are not designed for these extreme conditions (Fig. 4.4). The $Mn_{1.5}Co_{1.5}O_4$ coating

reduced the corrosion rate of Crofer 22A and 430 alloys by a factor of 10 compared to the uncoated alloys at 800°C, whereas on the 441 alloys the effect of the $Mn_{1.5}Co_{1.5}O_4$ coating is less pronounced due to a poor oxide scale adhesion (Fig. 4.4). Interestingly, there is not much difference in the corrosion rate values at lower temperatures for uncoated and $Mn_{1.5}Co_{1.5}O_4$ coated alloys at lower temperature (700°C). Here the commercial alloy 430 performs comparable to Crofer 22APU.

For all alloys the corrosion rate is at least doubled in pure oxygen compared to air atmosphere (Fig. 4.4). In reducing atmosphere (humidified hydrogen) on the other hand the corrosion decreases by 50 %. Even if the corrosion rate is low in reducing atmosphere, microstructural analysis showed a significant Cr loss from the alloy, which could lead to breakaway corrosion after longer operation time. The protective coating currently used at HTAS prevents Cr volatilization but does not reduce the corrosion rate. Hence it is important to develop a good protective coating for humidified hydrogen atmosphere for SOEC applications. In air (or even oxygen) at temperature around 700 °C or lower the commercial alloy 430 in combination with the developed coating could be an interesting alternative on the long run.

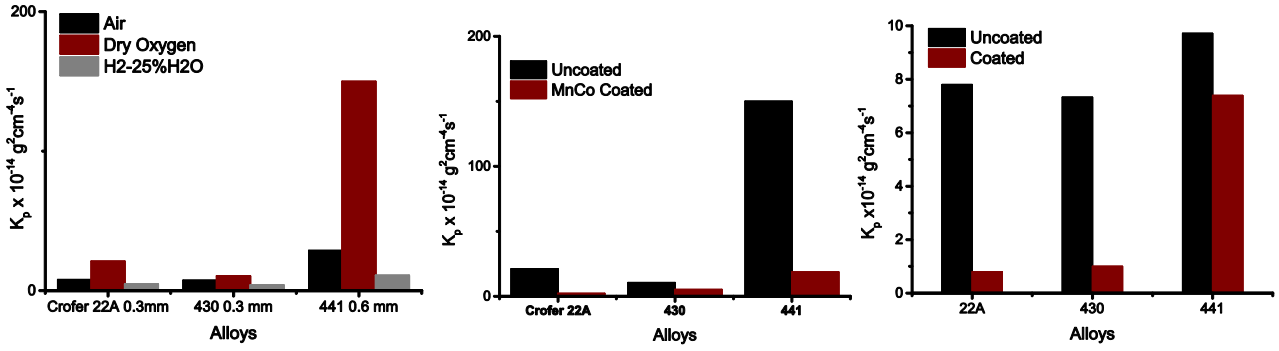

(a) *(b)* *(c)*

Figure 4.4: Corrosion rate (K_p) at 880 °C. Comparison of different alloys (a) in different atmospheres and with Mn-Co spinel coated in (b) pure dry oxygen at 800 °C after 1000 h and (c) air atmospheres at 800 °C after 1000 h.

ASR measurements (relevant to 4.4.3)

To additionally evaluate the electronic conductivity and therewith investigate the potential use in SOFC/SOEC, the area specific resistance of the alloys with and without Mn-Co spinel coatings was measured. To provoke a rather fast degradation, which is important to identify the long-term degradation mechanisms, the experiments were performed at 800 °C. During the measurements the samples were subjected to rapid cooling and heating after every 1000 hours to check their behavior during thermal cycling. The uncoated 430 alloys showed very high area-specific resistance (ASR) values of 1 $\Omega.cm^2$,

whereas 441 alloys showed only 0.2 Ω.cm^2, close to Crofer alloys (0.1Ω.cm^2) after 2500 hours (Fig. 4.5a). With the Mn-Co spinel coating both the 430 and 441 alloys showed very low ASR values (0.03 Ω.cm^2) similar to Crofer till 3000 hours in air at 800°C, but the ASR increased steadily during longer duration (Fig. 4.5b). As expected, the linear degradation rate increased significantly after 3000 hours for the Mn-Co spinel coated 430 and 441 alloys compared to the Crofer alloy (Fig. 4.5c). This shows that the commercial alloys could not maintain a low ASR during rapid thermal cycling at such high temperatures.

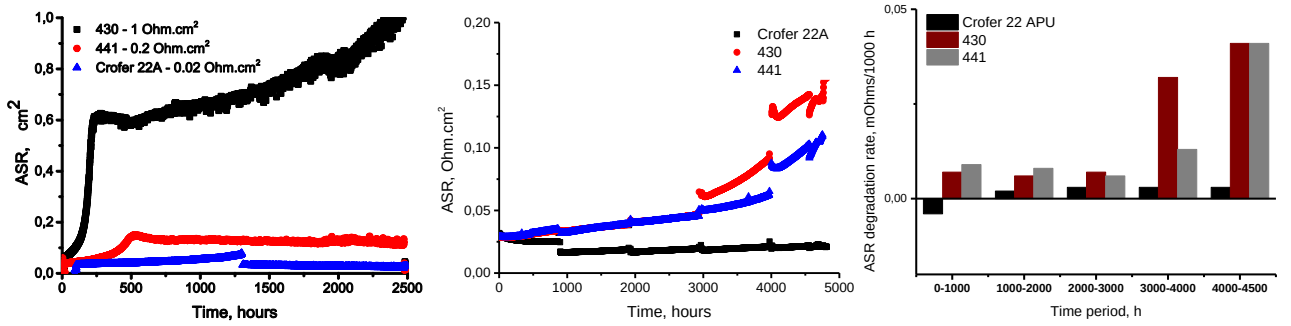

Figure 4.5: ASR measurements of different alloys (a) Uncoated, (b) with MnCo spinel coated at 800°C in air atmosphere, (c) Linear degradation rate of the Mn-Co spinel coated alloys at different time period

Modeling of Ni Diffusion Induced Austenite Formation in Ferritic Stainless Steel Interconnects (relevant to 4.41)

Summary: The inter-diffusion of Ni from the SOEC cells into the metallic interconnect was successfully modelled and compared to experimental data. This model will be extremely useful to predict the long-term stability of the IC steel (e.g. formation of austenitic phases) at the contact points to cell.

During stack production and operation, inter-diffusion across the cell – IC interface takes place, which under certain circumstances introduces adverse effects on the electrical, mechanical, and corrosion properties of the IC plates. One representative example is diffusion of nickel from the Ni/YSZ fuel electrode or from the Ni contact component into the IC plate, while iron and chromium from the steel diffuse in the reverse direction. Diffusion of Ni into the steel causes transformation of the ferritic BCC phase into the austenitic FCC phase in the interface region, accompanied with changes in volume and in mechanical and corrosion properties of the IC plates.

Very few studies have been devoted to investigate this process experimentally. In this work, kinetic modeling of the inter-diffusion between Ni and FeCr based ferritic stainless steel was conducted, using the CALPHAD (CALculation of PHAse Diagrams) approach with the DICTRA software. The kinetics of inter-diffusion and austenite formation was explored in full detail, as functions of steel composition, thickness of Ni contact component or IC plate, temperature and time. The simulation was further validated by comparing with previously obtained experimental results. The experimental results show that after 2000 h at 800°C Ni diffuses more than 100 µm deeper into Crofer 22 APU. DICTRA modeling gives a proper account

of the experimental results on inter-diffusion and accompanied $\alpha \rightarrow \gamma$ phase transformation, when both bulk and grain boundary diffusion are considered (Fig. 4.6). The inter-diffusion between Ni and Crofer 22 APU observed in the current work can be well explained by the thermodynamics and kinetics of the Fe-Cr-Ni system. The small amount of Mn in Crofer 22 APU seems to promote the $\alpha \rightarrow \gamma$ transformation slightly. DICTRA modeling further predicts enrichment of Mn towards Ni. The present work provides a proper account of the thermodynamics and kinetics of Ni-steel inter-diffusion and in addition provides input to further analysis of associated changes in the mechanical and corrosion properties of the IC plates.

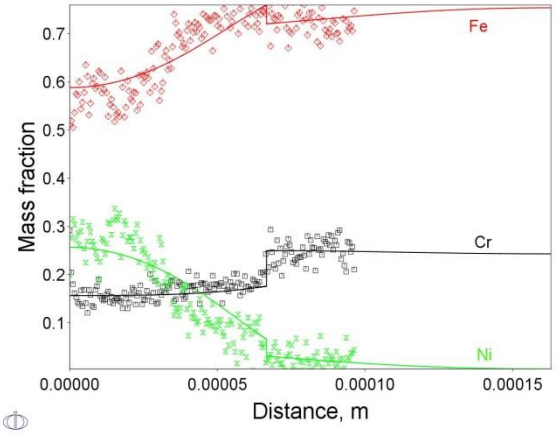

Figure 4.6. Calculated composition profiles (in mass fraction) along the diffusion couple of Ni – Fe0.77Cr0.23 heat treated at 800 °C for periods up to 2000 h. The initial thickness was 13 µm and 150 µm for the Ni and $Fe_{0.77}Cr_{0.23}$ layers, respectively. Both bulk and grain boundary diffusion are considered. The experimental data points are from the present work. Mn was excluded in calculating mass fraction.

5.2 WP 5 "Cells"

Overview milestones and deliverables in WP5. Deliverables already delivered and reported before change in the project structure due to TOFC closure are marked in **black**; deliverables (including new and modified ones) relevant for this reporting period are marked in **green**.

WP 5	
Deliverables (including modified and new ones)	
5.1.1	MTC cells for verification in stack: Half-cell series produced by multilayer tape casting delivery for stack testing in WP4 (Prototype series, M6) **Delivered**
5.1.2	Selection of manufacturing method: Report on method selection and cost of plasma coating, incl. cost development with volume (Report, M12) **Delivered**
5.1.3	Control of sintering: Recommendations for manufacture of cells with improved sintering shrinkage control and reduced edge curl (Report M21) **Delivered**

5.1.4	Cell yield improvements established and documented (Report M 23) **Delivered**
5.1.5	Net shaping: Mapping of cell shrinkage from selected cell geometries (Report M24) **Delivered**
5.2.1	First version of cathode backbone: First version cathode backbone tested with LSC and backbone cells delivered for cathode development in WP5.3 (Development cells M6) **Delivered**
5.2.2	Improved cathode backbone cells delivered for WP5.3 (Development cells M10) **Delivered** Comparable deliverable for SOEC cells added (New deliverable 5.2.5)
5.3.1	New cathode concept: Concept developed and sample cells delivered for durability tests (Test cells M15) **Delivered**
5.3.2	Prototype cell batch: Manufactured according to new cathode concept for stack testing in WP4 (Prototype series M20) **Delivered**
5.3.3	Improved cathode concept: Concept developed and sample cells delivered for durability tests (Test cells M18) **Delivered** Comparable deliverable for SOEC cells added (New deliverable 5.2.4)
5.3.4	Improved prototype batch: Manufactured according to cathode concept for stack testing in WP4 (Prototype series M21) **Delivered** Comparable deliverable for SOEC cells added (New deliverable 5.3.5)
New deliverables from DTU	
5.1.6	MTC cells for verification in stack: Half-cell series produced for stack testing under SOEC conditions in WP4 (Prototype series, M24) **Delivered**
5.1.7	Net shaped cell tested in single cell test under SOEC conditions (prototype cell M28) **Delivered**
5.2.3	Mechanical properties of new cathode backbone cells tested at relevant temperatures (Report M30) **Delivered**
5.3.5	Improved cathode backbone cell tested under SOEC operation conditions (report, M28) **Delivered**
New deliverables from HTAS	
5.1.8	10 m of Anode and electrolyte MTC tape delivered to DTU for net shaping experiments (casted tapes, M22 **Delivered**
5.1.9	10 m of Anode support tape delivered to DTU for net shaping (casted tapes, M22) **Delivered**
5.2.4	25 cells with newly developed cathode backbone delivered to DTU for cell testing in electrolysis mode (Development cell, M22) **Delivered**
5.2.5	25 half cells with cathode backbone structure delivered to DTU for mechanical testing (Development cell, M22) **Delivered**
5.2.6	3.5 m of cathode backbone tape delivered to DTU for thermo-mechanical analysis (casted tapes,

	M22) **Delivered**
5.3.6	15 m (thickness 10 um and 30 um) of E-glass felt delivered to DTU for sealing for cell testing (glass felt, M 22) **Delivered**
5.3.7	LNC Infiltrated samples for BET measurements delivered to DTU (powder, M22) **Delivered**
5.3.8	Report on time dependence of BET and conductivity of LNC infiltrated backbone material delivered to DTU (report, M24) **Delivered**
New milestones for work package 5	
M4	Title: *Net shaped cell manufactured according to specification for single cell test.* Description: A single cell with the dimension of 5.3×5.3 cm is manufactured using net shaping. The sintered cell will be tested without further shaping (e.g. laser cutting) in a single cell test. The performance test will show that the cell is robust and flat enough so it can be sealed according to standard procedure. Time: M28 **FULFILLED**
M5	Title: *Mechanical stability of cathode backbone cell demonstrated.* Description: The mechanical strength of the new cathode backbone cells will be measured at room temperature and SOEC operation temperature. The results will be compared with similar data from standard production cells. Time: M30 **FULFILLED**
M6	Title: *Stability of new cathode concept demonstrated under SOEC conditions (proof-of-concept)*. Description: A cathode backbone cell with an infiltrated electro catalyst will be tested for >1000 h under SOEC conditions (-0.5 A/cm^2 @ 800 °C). The performance is expected to be comparable or better than a standard cell. Time: M28 **FULFILLED**

5.1 Half-cell concept and process

Net shaping: Mapping of cell shrinkage from selected cell geometries (relevant to D5.1.3 and D5.1.5)

Summary: Net shaped cells in different sizes and shapes were successfully produced using a compensation layer. Together with an optimized sintering profile undesired feature like edge curl or wrapping are avoided and flat cells, which do not need any further shaping, can be obtained.

The following description of optimized design of solid oxide cell by compensation layer (net shaped cell) is based on the DTU owned patent WO2015059166 and was significantly improved during this project.
For ceramic materials, especially shaped as multilayer, de-binding and sintering are critical processes due to the effects of organic additives removal, material densification by solid state diffusive phenomena, and shrinkage mismatch of the layers. These processing steps can easily lead to critical shape instabilities and deformation. In order to obtain flat cells, a compensation layer or frame can be laminated to the half-cell on the anode support side. (Figure 5.1).

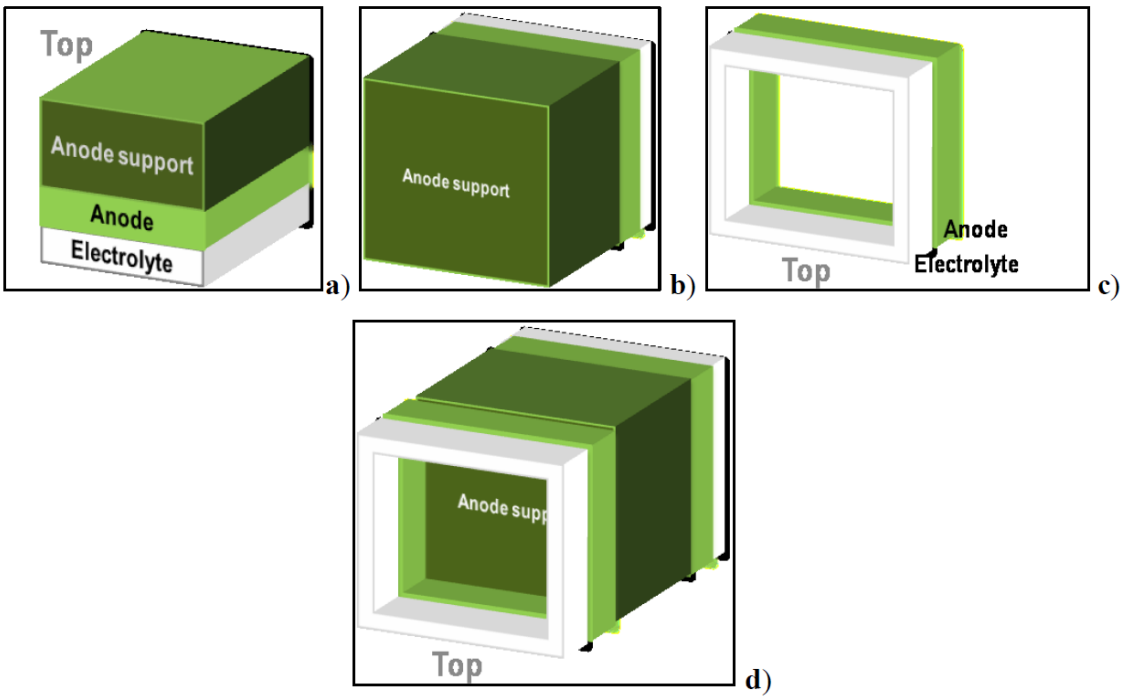

Figure 5.1. Uncompensated cell: a) half cell side view. b) half cell top/side view. c) Anode/Electrolyte frame. Compensated net-shaped cell: d) framed cell final configuration.

Using this method, flat cells in different sizes (e.g. 5×5 cm^2 for single cell testing in D5.1.6 or 12×12 cm^2 for potential use in stacks) and shapes (square, rectangular or triangular Fig 5.2) were obtained. As reported in D5.1.6, these cells can be directly used and tested without further shaping. Undesired features like edge curls or wrapping can be eliminated with this method and the optimized sintering profile. Also round holes with a diameter up to 15 mm), which are needed for internal gas distribution in a stack, were successfully added to the compensated structure (Fig. 5.3) without the need of shaping the sintered cell.

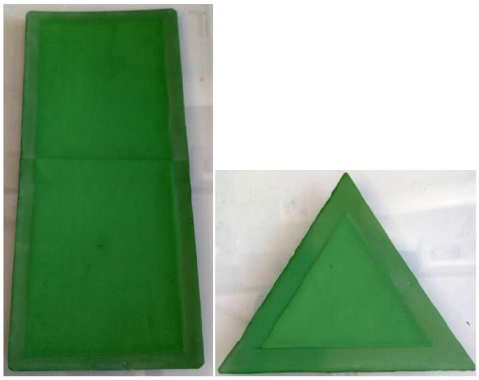

Figure 5.2 Framed cell with different shapes

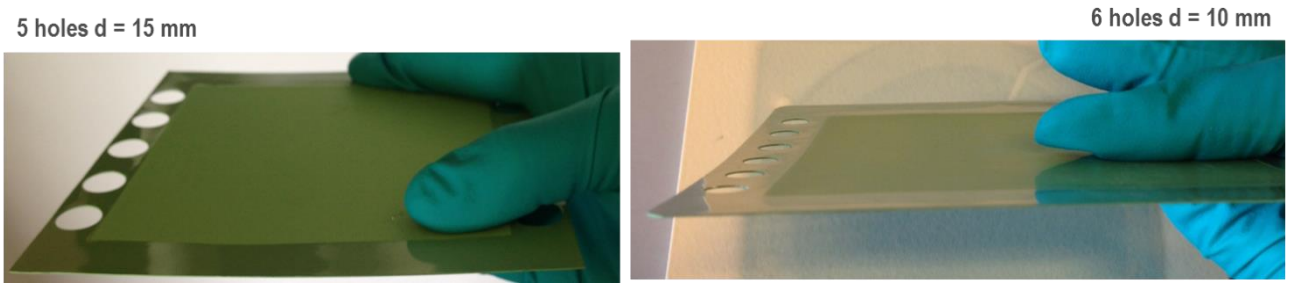

Figure 5.3 Framed cell with compensation layer and holes

It is recommended to further investigate the properties of these cells in regards mechanical stability and performance and to develop scale-up the production and finally test them in a SOEC/SOFC stack.

Net shaped cell tested in single cell test under SOEC conditions (relevant to D5.1.5, D5.1.7 and M4)

Summary: A net shaped cell was produced and successfully tested in SOFC/SOEC operation. The sealing and testing procedure was according to standard protocol, no further shaping steps were used.

A single anode-supported cell with the dimension of 5.3×5.3 cm^2 manufactured using net shaping was tested without further shaping (e.g. laser cutting) in a single cell test. LSM/YSZ was applied by screen printing as oxygen electrode with an additional layer of LSM as current collector. This oxygen electrode was used to prove the concept and the usability of the net-shaping procedure. The test (Fig. 5.4) showed that the cell is robust and flat enough to properly seal the fuel electrode by using the setup and procedure used at DTU Energy.

The initial cell voltage obtained with 4 % H_2O + 96 % H_2 supplied to Ni-YSZ electrode and air to the LSM/YSZ electrode at 850^oC was ca. 1067 mV (theoretical value 1076 mV). The cell performance is comparable to state-of-the-art SOFC cell with a comparable cathode; using a more advanced state-of-the-art oxygen electrode (e.g. LSCF/CGO with CGO barrier layer) could increase the performance of this type of produced cells.

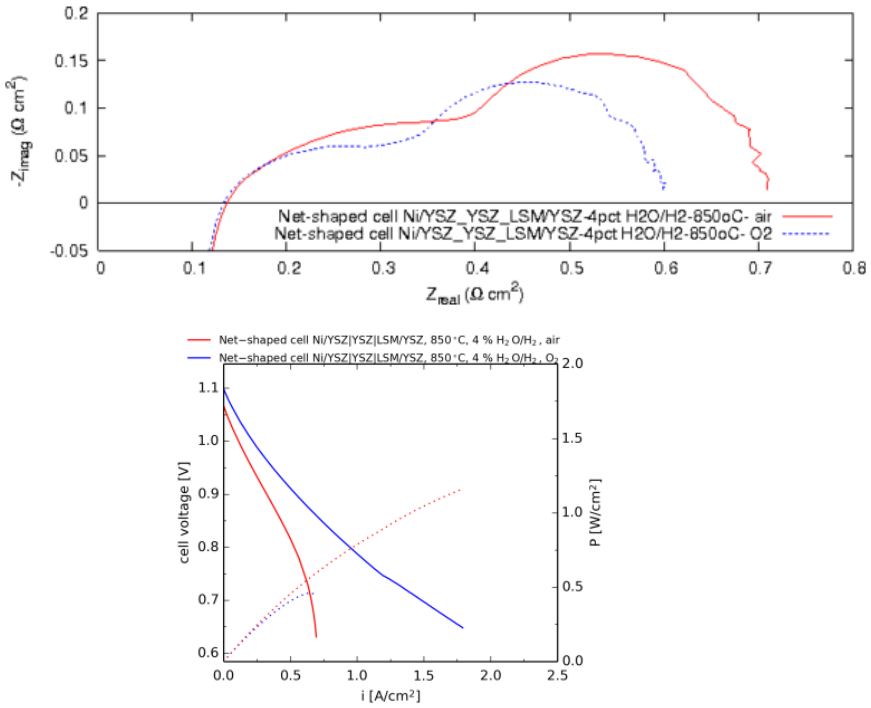

Figure 5.4: Electrochemical measurements of the net-shaped cell at 850 °C, 4% H_2O/H_2 at the fuel-electrode, air or O_2 at the oxygen electrode. Left) EIS Nyquist plots. Right) Equivalent conditions iV-curves.

5.2 Novel cell design – cathode backbone cells

Development and optimization of a cathode backbone cell (relevant to D5.2.4, D5.2.5, D5.2.7)

Summary: Cells of a novel design called the "cathode backbone cells" or "EUDP cells" have been developed within the project. The new cells offer a lower-cost alternative to currently used so-called DTU/HTAS 2.5G cells. It was shown that cathode backbone cells can be produced with reasonable yields in pilot production batches of 90 cells. The sintered blank cells (see Fig. 5.5) were delivered to DTU for infiltration and further mechanical and electrochemical testing.

A new cell design consisting of the traditional NiO/YSZ support, NiO/YSZ anode, YSZ electrolyte and novel cathode, made by infiltrating nitrate precursor solutions into a porous YSZ cathode backbone layer, was developed in the project. The development of the backbone layer and that of the cell fabrication process was developed at TOFC/HTAS as part of WP5.2. The development of the subsequent infiltration step was pursued jointly by HTAS and DTU.

The procedure for the fabrication of the novel cathode backbone cells was developed within the EUDP project and is described in two European patent applications filed by TOFC (and inherited by HTAS): EP13171699 and EP13171700. Compared to the processing of current state-of-the-art "DTU/HTAS 2.5G cells", the new cell can be manufactured in fewer high-temperature processing steps and makes use of relatively cheap nitrates compared to more expensive complex ceramic oxides in the cathode. Both of these improvements are expected to significantly reduce the price of the cell. A simplified schematic of the production process is provided in Fig. 5.5.

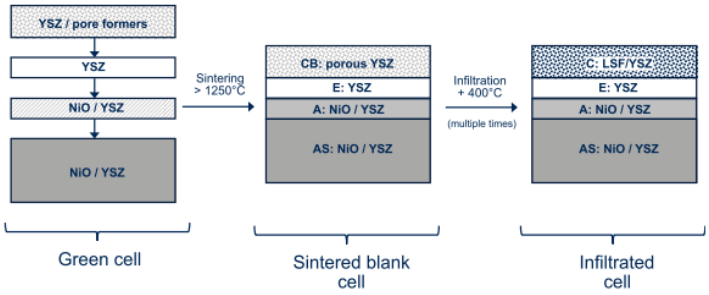

Figure 5.5: Steps in the manufacturing of the new "EUDP cells".

Optimizing the procedure described above, cell batches of up to 90 cells could be successfully manufactured at HTAS with a 75% yield. The obtained cell yield is deemed promising considering the novelty of the entire production process. Through future improvements and process optimization, much higher cell yields are possible.

Strength of cathode backbone cells (relevant to D5.2.3 and M5)

Summary: The mechanical strength of the new developed cathode backbone cell was measured at room temperature and under operation temperature. The mechanical strength is comparable to the strength of standard production cells.

The mechanical strength of cathode backbone cells was measured to ensure comparable mechanical robustness with standard production half-cells. The strength of unreduced cathode backbone cells was evaluated using four-point bending test at room temperature and operating temperature of 800°C in air. For each temperature, a total of 30 cathode backbone cells were fractured to obtain a statistical distribution of strength.

Residual stresses are present in the cells prior to testing due to the mismatch in thermal expansion coefficients of the different layers. The residual stresses were first calculated based on the measured curvature of the cells at room temperature and the thermo-elastic properties of the layers. Additional stresses arise upon application of load on the samples under four-point bending. The sum of the two contributions gives the total stress experienced by the cells. The calculated stress distribution reveals that the highest tensile stress is located at the anode support while the other layers experience compressive or insignificant tensile stress. The measured strengths thus correspond to that of the unreduced anode support.

The strength of the anode supports at room temperature and operating temperature are shown in Fig. 5.6. The statistical distribution of strengths was analyzed with the standard Weibull theory, and the corresponding Weibull parameters are summarized in Table 1. The effective volume was computed to be 0.4 cubic millimeters. The Weibull parameters of standard production half-cells at room temperature have been measured with the ball-on-ring method in a separate study (*Journal of Power Sources,* **288** (2015) 243-252), which reported Weibull strength of 394 MPa at an effective volume of 0.34 and Weibull modulus of 17.2. The measured strength properties for cathode backbone cells shown in Table 5.2 are in close agreement with those of standard production half-cells. It can therefore be concluded that the cathode backbone cell has maintained the same mechanical strength of the standard production cells. A lower

Weibull strength was measured at 800 C. The strength reduction is attributed to the reduction of elastic modulus with temperature.

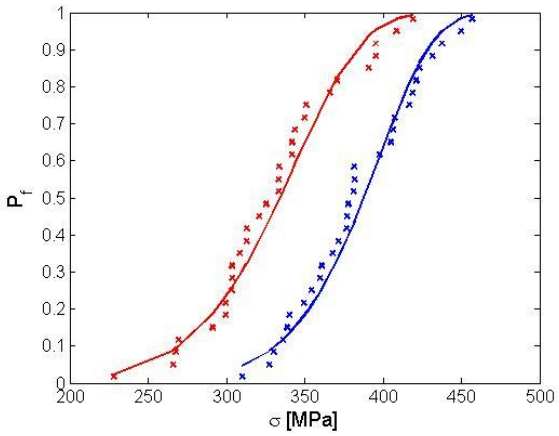

Figure 5.6 Fracture probability distributions of anode supports in cathode backbone cells at 800 °C (red) and 30 °C (blue)

Table 5.2 Summary of strength parameters measured for cathode backbone cells.

	Weibull strength [MPa]	Weibull modulus
T = 30°C	399.8	12.0
T = 800°C	348.2	8.8

5.4 Cathode material

Long-term stability of infiltrated cathodes (relevant to D5.3.7, D5.3.8)

Summary: The stability of infiltrated cathodes was evaluated by measuring the in-plane conductivity and electrode active surface area as a function of the time the samples were exposed to 750°C, 850°C, or 900°C. The conductivity of the samples decreased steadily with time, but the surface area (and thus the particle size) of the electrode active material remained surprisingly stable even after 5000 hour treatment at 750°C.

Cells with novel infiltrated porous zirconia backbone cathodes were fabricated and aged for up to 5000 hours at HTAS. Changes in the in-plane conductivity of the infiltrated electrodes were monitored by regular van der Pauw conductivity measurements at 700°C. The conductivity of the infiltrated electrodes decreases as the sample is aged. This effect is accelerated at higher temperatures.

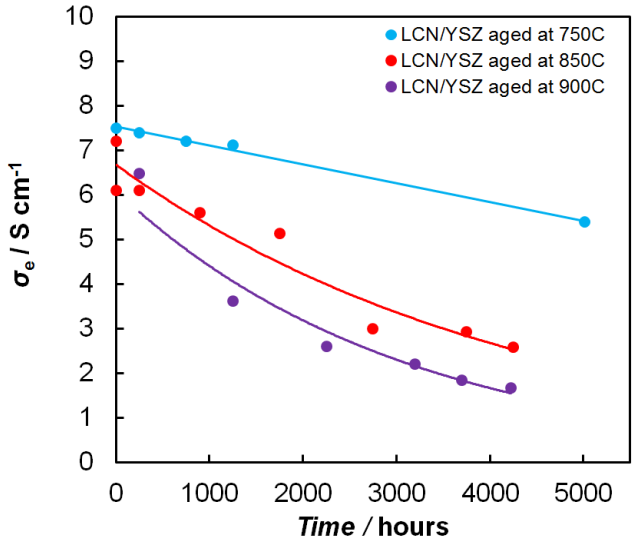

Figure 5.7 In-plane conductivity of cathode backbone cells infiltrated with $La_{0.95}Co_{0.4}Ni_{0.6}O_3$ (LCN), aged for up to 5000 hours at 750°C (blue symbols), 850°C (red symbols), and 900°C (purple symbols).

Simultaneously, pieces of infiltrated porous zirconia backbone were aged in the same conditions and characterized regularly for changes in specific surface area and pore-size distribution using BET N_2 adsorption method. The specific surface area of the samples aged at 850°C and 900°C decreases as the samples are aged, but the rate of sintering seems to slow down with time. Most notably, the sample pre-calcined to 850°C and then aged at 750°C retains 95% of its original surface area after 3600 hours of aging. These results can help to interpret the excellent stability of the cell tested in SOEC mode (see next section).

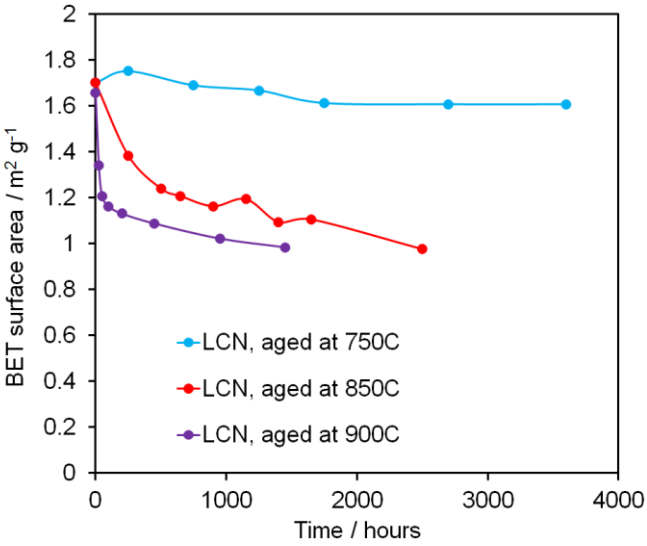

Figure 5.8 Specific surface area of cathode backbone samples infiltrated with $La_{0.95}Co_{0.4}Ni_{0.6}O_3$ (LCN), aged for up to 5000 hours at 750°C (blue symbols), 850°C (red symbols), and 900°C (purple symbols). Note the stability of the sample aged at 750°C.

Improved cathode backbone cell tested under SOEC operation conditions (relevant to D5.3.5 and M6)

Summary: The infiltration procedure for obtaining high performance cathodes was further optimized and a reproducible manufacturing procedure was established. The cells were long-term tested under SOEC conditions and excellent cell performance and long-term stability was obtained.

Cathode backbone cells were first infiltrated with a precursor solution of metal nitrates corresponding to $Ce_{0.8}Gd_{0.2}O_{1.9}$. Different surfactants and infiltration processes were studied to improve the covering of the backbone with a CGO barrier layer to prevent direct contact between the YSZ and the electrocatalyst.
After the CGO infiltration, the cathode backbone cells were infiltrated 11 times with a precursor solution of metal nitrates corresponding to nominal composition of $La_{0.95}Co_{0.4}Ni_{0.6}O_3$ (LCN). The infiltration procedure was varied to achieve a high loading of electrode catalyst in the backbone, prevent the clogging of pores and to form a current collector layer on the surface of backbone.
The SEM micrographs in Figure 5.9 provide overview of the cross section of the infiltrated cathode backbone cell before long term testing. The magnified image shows in greater detail that the YSZ backbone is evenly covered with a CGO barrier layer. Another noticeable feature is the layer on the surface of backbone. This layer is composed of LCN that has not been completely infiltrated into the backbone and serves as a current collector layer (CCL). Therefore the additional screen printing of the CCL, which is frequently used in a cell production, is not necessary for the infiltrated backbone cells.

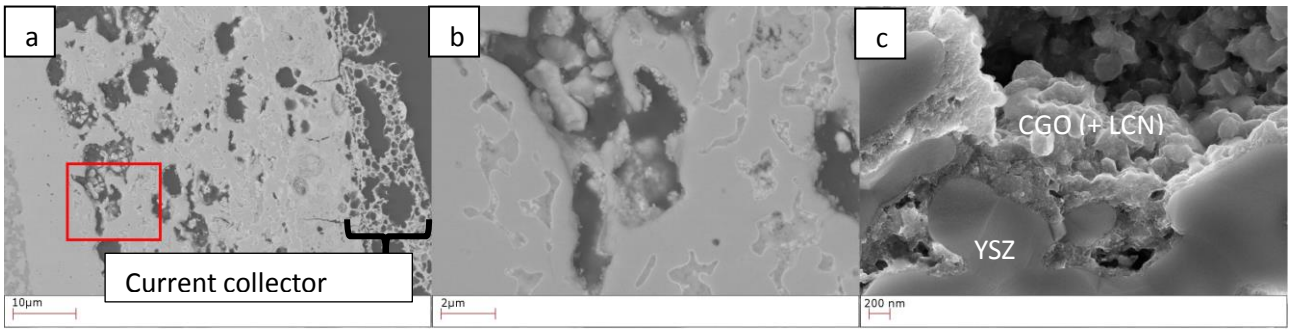

Figure 5.9: SEM micrographs of a+b) polished cross section and c) fractured cross section in vicinity of electrolyte of infiltrated cathode backbone cell.

The SOEC performance of the LCN infiltrated cathode backbone cell was tested with 40 l/h O_2 supplied to the oxygen electrode and 90% H_2O + 10% H_2 at a rate of 13.4 l/h supplied to the Ni/YSZ-electrode, ca. 60 % conversion. The cell voltage was recorded under a constant applied current of -1 A/cm^2 at 800 °C for more than 2000 h.
The performance of cell was compared with the standard cell tested under the same conditions. For the standard cell TOFC 2.5G with Ni/YSZ|YSZ|LSCF and screen printed LSM current collector layer was used.
The cell voltage for infiltrated cathode back bone cell and standard cell as function of time at 800 °C under a constant applied current of -1 A/cm^2 are shown in Figure 5.10. Higher cell voltage is measured for the standard cell than for the infiltrated cathode backbone cell. The cell voltage of the standard cell and the cathode backbone cell stabilizes after ca. 200h and ca. 600h, respectively. After 1000 h of cell testing, the activation of the cell is observed and final cell voltage after 2200 h is ca. 1202 mV. Comparatively, the performance of the cathode backbone cell is overall better than the standard cell. From the EIS and R_p and R_s splitting of the infiltrated backbone cell during testing, it can be estimated that the R_p reaches a stable resistance, whereas R_s linearly increases. From these estimations it seems that it may be able to run almost 3 years uninterrupted before reaching a critical cell voltage of 1500 mV.

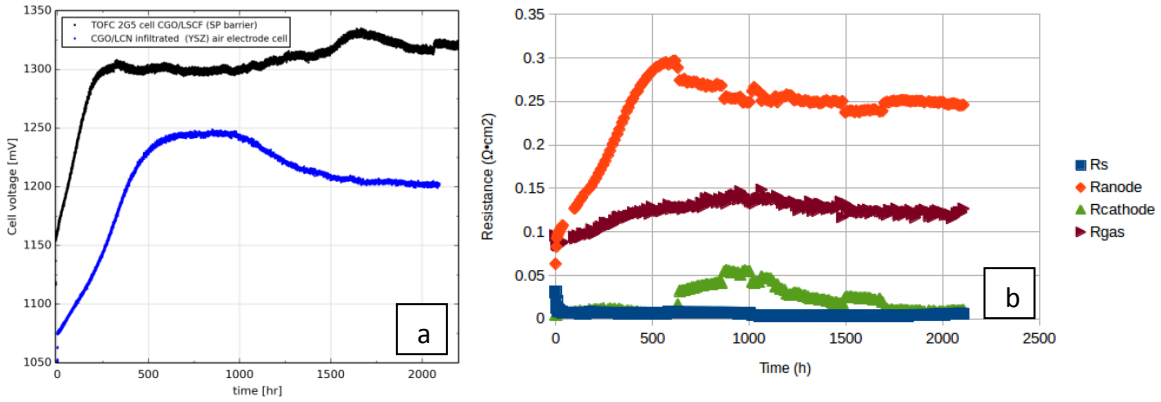

Figure 5.10: a) Cell voltage evolution over time during constant operation at 800 °C under a constant applied current of -1 A/cm^2 for a standard TOFC 2.5G cell and a CGO/LCN infiltrated cathode backbone cell. b) Deconvolution of the electrochemical impedance spectra for the CGO/LCN infiltrated cathode backbone cell.

From the deconvolution in figure 5.10b, it can be noted that the initial resistance increase can be attributed to the anode (fuel electrode), at ca. 600h the cathode (air electrode) increases in resistance contribution, which peaks at ca. 1000h, after which it also activates. After ca. 1800, the serial resistance seems to linearly increase.

It should be emphasized that to our knowledge neither such a high performance nor such excellent long term stability has been reported for a SOEC cell until today. Therefore further development and testing on stack level is recommended.

5.3 Dissemination

Published in peer reviewed journals and proceedings (articles submitted or under internal review included):

1) D. Marani, C. Gadea, J. Hjelm, P. Hjalmarsson, M. Wandel, R. Kiebach *"Influence of hydroxyl content of binders on rheological properties of cerium–gadolinium oxide (CGO) screen printing inks"*, Journal of the European Ceramic Society 35 (2015) 1495–1504.

2) D. Marani, B. R. Sudireddy, J. J. Bentzen, P. S. Jørgensen, R. Kiebach *"Colloidal stabilization of cerium-gadolinium oxide (CGO) suspensions via rheology"*, Journal of the European Ceramic Society 35 (2015) 2823-2832

3) D. Marani, B. R. Sudireddy, R. Kiebach, L. Nielsen, S. Ndoni *"Poly (vinylpyrrolidone) as dispersing agent for cerium-gadolium oxide (CGO) suspensions. Effect of molecular weight characteristics"*. Journal of Material Science.

4) D. Marani, B. R. Sudireddy, J. J. Bentzen, P. S. Jørgensen, F. Teocoli, D. Ni, V. Esposito, R. Kiebach *"Fabrication of dense thin cerium-gadolinium-oxide (CGO) electrolyte"*, Journal of the European Ceramic Society.

5) S. Veltzé, S. Ovtar, Y. Xu, S. Bredmose Simonsen, K. Kwok, H. Lund Frandsen, A. Samson, R. Küngas, R. Kiebach, *"Combining robustness and simplicity with high performance: Design, performance and long-term stability of anode supported SOFC with a co-sintered cathode backbone and infiltrated $LaCo_{0.4}Ni_{0.6}O_3$ (LCN) electro-catalyst"*, ChemSuSChem.

6) S. Ovtar, R. Kiebach, M. Chen, A. Junio Samson *"In-situ formed $Ce_{0.8}Gd_{0.2}O_{1.9}$ barrier layer on yttria stabilized zirconia back-bone for lanthanum cobalt nickelate infiltrated cathodes"*. Journal of Materials Chemistry A.

7) F. Teocoli, R. Kiebach, V. Esposito, "*Effect of porosity on cambering of co-fired dense/porous zirconia thin bi-layers",* Journal of European Ceramic Society.

8) R. Kiebach, P. Zielke, J. Valdemar Thorvald Høgh, K. Thydén, J. Wang, R. Barford, P. Vang Hendriksen, "*Infiltration of SOFC stacks: Evaluation of the electrochemical performance enhancement and the underlying changes in the microstructure"*, Fuel Cells.

9) V. Venkatachalam, S. Molin, M. Chen, P.V. Hendriksen, R. Kiebach, „*Evaluation of commercial ferritic stainless steels with $Mn_{1.5}Co_{1.5}O_4$ coating for SOFC interconnects applications using Electrophoretic deposition",* Journal of Power Sources.

10) P. Zielke, R. Rode Mosbæk, J. Høgh, R. Barfod, P. Vang Hendriksen, Johan Hjelm, *"Impedance Based Solid Oxide Fuel Cell Stack Diagnostics"*, Fuel Cells.

11) V. Venkatachalam, S. Molin, R. Kiebach, M. Chen, P.V. Hendriksen, "*Evaluation of commercial ferritic steels as interconnects under SOEC conditions*" Journal of Power Sources.

Conferences

1) D. Marani, B. Reddy Sudireddy, R. Kiebach, L. Nielsen, S. Ndoni**,** "Rheological properties of poly (vinylpiyrrolidone) as a function of molecular weights", Annual Transaction of Nordic Rheology Conference, 22 (2014) 11-18.

2) D. Marani, B. Reddy Sudireddy, R. Kiebach, L. Nielsen, S. Ndoni**,** "Rheological properties of poly (vinylpiyrrolidone) as a function of molecular weights", 1st Annual World Congress of Smart Materials-2015, Busan, Republic of Korea (invited).

3) M. Chen, S Molin, L. Zhang, N. Ta, P. Vang Hendriksen, R. Kiebach, Y. Du "*Modeling of Ni Diffusion Induced Austenite Formation in Ferritic Stainless Steel Interconnects"* ECS Conference on Electrochemical Energy Conversion & Storage with SOFC-XIV (July 26-31, 2015) in Glasgow.

4) R. Küngas, T. B. Hertz, T. Heiredal-Clausen, *"Characterization and Stack Testing of Solid Oxide Fuel Cells with Cathodes Prepared by Infiltration"*, ECS Conference on Electrochemical Energy Conversion & Storage with SOFC-XIV (July 26-31, 2015) in Glasgow.

5) P. V. Hendriksen, M. Chen, R. Kiebach, X. Sun, K. Agersted, Y-L. Liu, S. Molin, S.D. Ebbesen, C. Graves, A. Hauch, K. Brodersen, M. B. Mogensen, J. Hjelm, S.H. Jensen, C. Chatzichristodoulou, B.V. Mathiesen, *"Prospects and Challenges of Solid Oxide Electrolysis"*, 20th International Conference on Solid State Ionics, June 14–19, 2015, Keystone Resort & Conference Center, Keystone, CO, USA.

6) V. Venkatachalam, S. Molin, W. R. Kiebach, M. Chen, P.V. Hendriksen, Influence of Mn-Co- spinel coating on oxidation behavior of ferritic SS alloys for SOFC interconnect applications, Materials Science and Technology (MS&T) October 12-16 2014, Pittsburgh, Pennsylvania, USA.

Patent applications

1) R. Küngas, K. K. Hansen, S. Kjølby, U. Rahbek, S. Primdahl, Electrochemical cell, EP13171699.
2) R. Küngas, K. K. Hansen, S. Kjølby, U. Rahbek, S. Primdahl, Impregnation of an electrochemical cell cathode backbone, EP13171700.
3) US 2014/0193743 Planar half-cell shaped precursor body
4) Esposito, V, Linderoth, S. Planar half-cell shaped precursor body, WO2015059166, 2015.